JOURNAL OF MATERIALS SCIENCE 11 (1976) 2287–2296

The formation and crystallization of an amorphous phase in an iron-carbon alloy

P. G. BOSWELL, G. A. CHADWICK
Department of Mining and Metallurgical Engineering, University of Queensland, St. Lucia, Queensland 4067, Australia

Splat-cooled foils of a carburised high purity Fe-C alloy have been examined by transmission electron microscopy. The crystalline phases that arose with an Fe $\simeq$ 4.3 wt % C amorphous phase on quenching and those that nucleated from the amorphous phase on heating were identified. The former was the HCP solid solution ϵ-phase whereas the latter, termed MS-I and MS-II, developed via two independent reactions yielding single phase ferrite grains and generally ferrite plus cementite grains, respectively. These observations have been interpreted in terms of the relative dispositions of transformation curves of the various metastable crystallization products.

1. Introduction

A non-crystalline phase has been reported to arise in conjunction with ϵ-phase grains in splat-cooled foils of an Fe–3.8 wt % C alloy [1]. However, special procedures were required in order to obtain a clean quenching substrate and the accompanying high heat-transfer coefficient at the foil-substrate interface. Crystallization of the amorphous phase occurred under beam heating in the electron microscope but the resulting structures were not described.

Davies *et al.* [2] have suggested that an amorphous phase may be produced in an alloy with a composition that is well removed from that with the highest glass-forming tendency, which probably has a composition close to that of the eutectic point at 4.3 wt % C in Fe–C alloys. If this is the case then it would be possible to compare crystallization structures with conventional reaction products of the decomposition of austenite. This is of interest because in Pd–Si alloys for instance, the MS-II crystallization stage that occurred on reheating the amorphous phase gave metastable phases with characteristic striations resembling those arising in internally twinned martensites [3]. However, little is known about martensitic structures in Pd–Si and most other glass-forming systems so comparisons with crystallization reactions cannot be made. On the other hand, Fe–C martensites are reasonably well characterized so if indeed it is possible to form an amorphous phase in a suitable alloy, comparisons may eventuate.

A second feature of splat-cooled Fe–C alloys, namely the reported presence of ϵ-phase grains in conjunction with the amorphous phase [1], is also of interest. In terms of kinetic models for glass formation on liquid quenching [2, 4], this observation implies that the production of an amorphour phase requires the suppression of significant ϵ-phase crystallization. On the other hand, it has been argued that the stability of the reheated amorphous phase is determined by different crystallization reactions so that the thermodynamic and kinetic factors controlling glass formation and stability are not the same [5]. Clearly a complete discussion of these two aspects requires the precise identification of crystal structures formed on quenching the melt and on heating the amorphous phase.

It was anticipated that there would be some difficulty in achieving the necessary cooling rate for the formation of an amorphous phase in splat-cooled Fe–C alloys if the normal procedures were adopted [6]. These procedures involve melting the alloys in an alumina crucible and the use of a carbon monoxide atmosphere to suppress the decarburization reaction between the melts and the crucible. The atmosphere probably reduces significantly the heat-transfer coefficient at the splat-substrate interface and the required cooling rates may not be realised. Shingu *et al.* [1] splat-cooled in a vacuum, thereby permitted decarburization to occur, but they were able to produce an amorphous phase. Given that some alteration of the alloy composition is unavoidable, it is more convenient to melt a low carbon alloy in a graphite crucible and to control the degree of carburization. This has the advantage that splat-cooled foils with a range of carbon concentrations can be readily obtained. There is also the possibility that any gradient of the carbon concentration within the melt may serve to facilitate droplet formation due to the reduced viscosity of the carbon-poor material. Since the thickness of the droplet after impact is proportional to the initial droplet diameter [7], any reduction in the average droplet size of the spray formed by a gun-type splat-cooling device would increase the probability of locating foil areas that had experienced the high cooling rates required for glass formation.

This communication describes the structures of as-quenched and reheated splat-cooled foils of an Fe $\simeq$ 4.3 wt % C alloy obtained after a specified carburization treatment. The crystalline phase in the two phase, crystalline plus amorphous structures that were observed in as-splatted material, was invariably the ϵ-phase. On the other hand, the reheated amorphous phase decomposed via the characteristic MS-I, MS-II crystallization stages, neither of which involved the nucleation and growth of the ϵ-phase. The implications of these results will be discussed in terms of the factors that govern glass formation and stability.

2. Experimental

A gun-type splat-cooling device was used to quench 200 mg molten charges of a high purity Fe-0.2 wt % C alloy onto a water-cooled, doubly-curved copper substrate. Both the gun and the substrate were contained in an evacuated chamber and the pressure waves for expelling the charges through a 1 mm diameter orifice were created by the rupture of 0.002 in. Mylar diaphragms with high purity argon. The charges were inductively heated in a high purity graphite crucible to 1900 ± 50 K and held at this temperature for varying lengths of time prior to splatting. The resulting foils were examined, without thinning, by transmission electron microscopy using a JEM200 STEM instrument operated at 200 kV. It was found that carburization times of 10 to 15 sec invariably gave foils with appreciable amounts of an amorphouse phase in electron-transparent regions so these foils were subsequently examined in more detail, both by electron microscopy and X-ray powder diffractometry. Fragments of the same foils were also examined during and after beam and hot stage heating in the electron microscope.

3. Experimental results

3.1. As-quenched microstructures

3.1.1. X-ray diffractometry

X-ray diffractometry of foils resulting from a 10 to 15 sec carburization treatment revealed a complex set of co-existing crystalline phases but ferrite, cementite, ϵ-phase [6] and austenite reflections could be detected. There were no indications of the presence of non-crystalline phases.

3.1.2. Transmission electron microscopy

While it was necessary to examine every foil by transmission electron microscopy for the presence of an amorphous phase, the results presented hereafter refer only to the foils resulting from the 10 to 15 sec carburization treatment. These foils revealed electron-transparent areas comprising lath martensite, twinned martensite, austenite grains, ϵ-phase grains, crystalline grains plus an amorphous phase and an amorphous phase. This progression in structures is thought to reflect the influence of solidification at progressively higher cooling rates. However, the dual presence of significant amounts of lath martensite, which is generally formed in low carbon material ($<$ 0.6 wt % C [8], and of the ϵ-phase, which has only been reported to arise in splat-cooled foils with more than 2.1 wt % C [6], indicate that the foil composion may not be uniform. This is surprising in view of the extremely rapid diffusivity of carbon in liquid Fe–C alloys. Whatever the origin of this

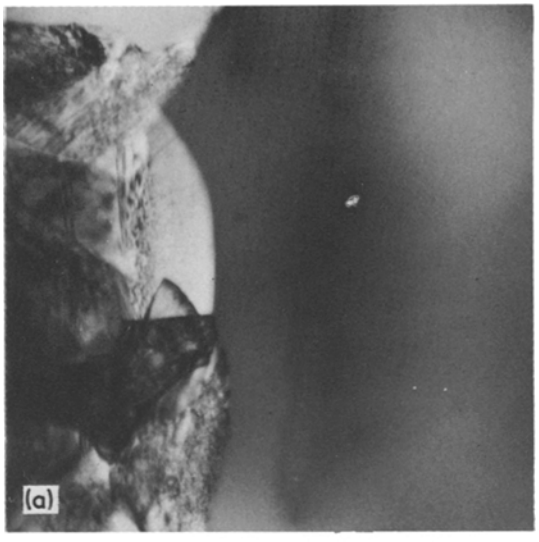

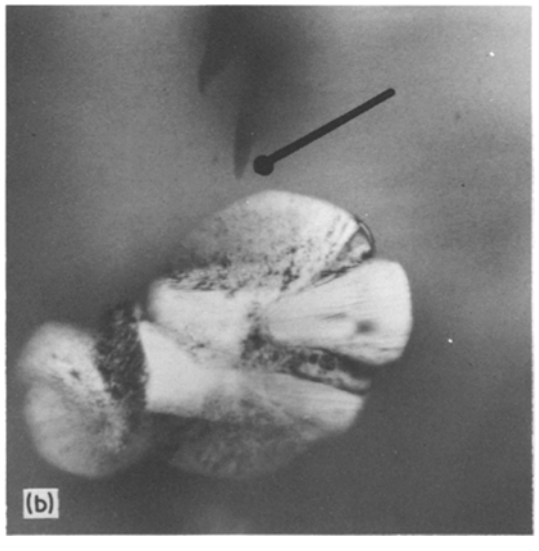

Figure 1 Bright-field transmission electron micrographs of ϵ-phase grains (a) bordering (× 42 000) and (b) embedded in (× 58 000), an amorphous phase in a splat-cooled Fe–C foil. Note indicated foil imperfection in (b).

effect, it was thought that the examination of totally crystalline structures would be misleading in the context of the aims of this investigation. Consequenctly, attention was only focussed on two morphologies, namely the amorphous regions and the amorphous plus crystalline regions. Examination of the former as-quenched microstructures should indicate the reactions that must be suppressed on cooling Fe–C alloys in order to form the amorphous phase.

3.1.2.1. Partially crystalline microstructures. The only crystalline phase that could be found in conjunction with the amorphous phase was the hexagonal ϵ-phase [6] which generally arose as rims of faulted grains around the peripheries of electron-transparent non-crystalline regions (Fig. 1a). Occasionally however, clusters of the faulted grains were observed to be embedded within the amorphous phase (Fig. 1b). The grain boundaries of the peripheral ϵ-phase were often normal to the ϵ-amorphous phase interfaces, indicating that these grains were growing into the non-crystalline phase from the surrounding thicker material.

3.1.2.1. Non-crystalline regions. Electron-transparent totally non-crystalline areas were frequently observed throughout small droplets that were attached by small bridges of material to the bulk of the foil. They could also be detected at the edges and interiors of large foil areas which were presumably made up of overlapping droplets. The microdensitometer trace (Fig. 2b) taken from the selected-area diffraction pattern (Fig. 2a) that was produced by a typical non-crystalline area reveals a definite inflexion on the high diffraction angle side of the second peak. It is anticipated that this feature would give a characteristic property of the interference function of metal-metalloid glasses [9], namely a pronounced shoulder on the second peak.

3.2. Decomposition on heating in the electron microscope

Beam heating for 5 min at 200 kV with the condenser aperture removed did not give significant decomposition of the partially or totally non-crystalline regions. A calibrated hot stage was therefore used to study the transformations of typical ϵ plus non-crystalline and non-crystalline foil areas. Heat-treatments were limited to a few minutes in order to prevent foil contraction and the reported transformation temperatures correspond to the temperatures required for about 10% transformation after 30 sec following heating to temperature at 5 to 10 K sec^{-1}. The indicated transformation temperatures are probably only accurate to within ± 10 K.

3.2.1. ϵ-phase

The ϵ-phase decomposed above about 430 K to small ϵ-carbide precipitates in a BCT ferrite matrix,

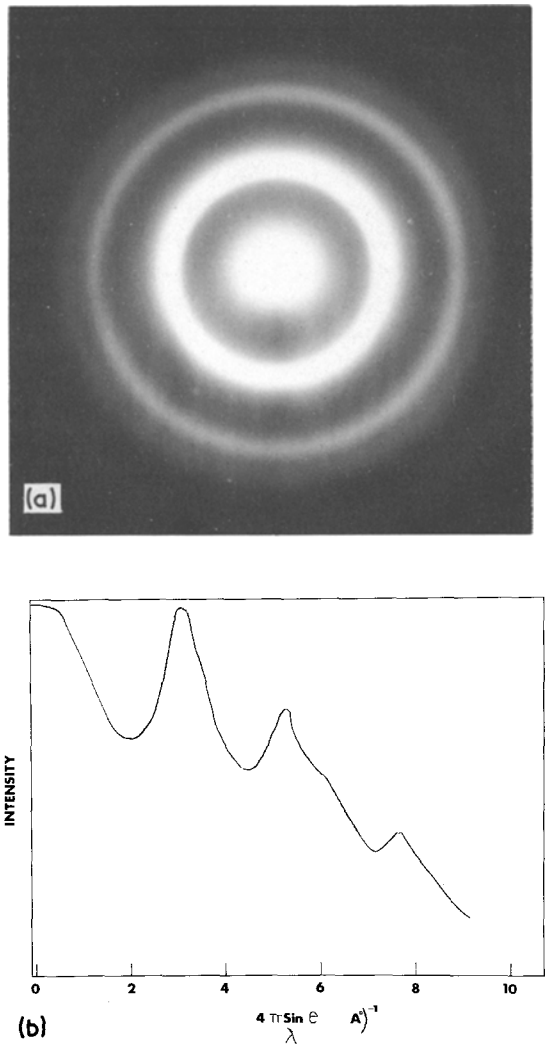

Figure 2 Typical selected-area diffraction pattern (a) and microdensitometer trace (b) produced by the amorphous Fe–C phase.

in agreement with Ruhl and Cohen's X-ray results which showed that this transformation took place within 1 h at temperatures between 410 to 470 K [6].

3.2.2. ϵ plus amorphous regions

It was noted that the amorphous ϵ-phase boundaries moved into the amorphous phase during heating at temperatures above about 470 K. Fig. 3 shows the same area as Fig. 1b after heating at $\simeq$ 510 K for 20 sec and the indicated foil imperfection can be used to compare the position of the ϵ-phase boundary before and after heating. The boundary has apparently moved at an average velocity of $\simeq 1.0\,\mathrm{nm\,sec^{-1}}$. However, it is important to realize that due to ϵ-phase decomposition, a two-phase BCT ferrite plus ϵ-carbide grain, rather than a undecomposed ϵ-phase, has grown into the amorphous matrix.

3.2.3. Amorphous phase

A characteristic two stage crystallization reaction was observed on reheating the amorphous phase to temperatures above about 480 K. It will be shown that these stages correspond to the MS-I and MS-II transformations described by Masumoto and Maddin for a $Pd_{80}Si_{20}$ amorphous alloy [3] and by Masumoto and Kimura for an $Fe_{80}P_7C_{13}$ alloy [10, 11].

3.2.3.1. MS-I reaction. The amorphous phase initially crystallized above 480 K by the copious random nucleation and subsequent growth of ferrite grains. A typical bright-field transmission electron micrograph taken during this reaction is shown in Fig. 4. The accompanying SADP reveals rings of diffracted intensity arising from the b c c ferrite which has a lattice parameter of 0.287 ± 0.002 nm. No preferred orientation arose and the ferrite grains became faceted at large grain sizes.

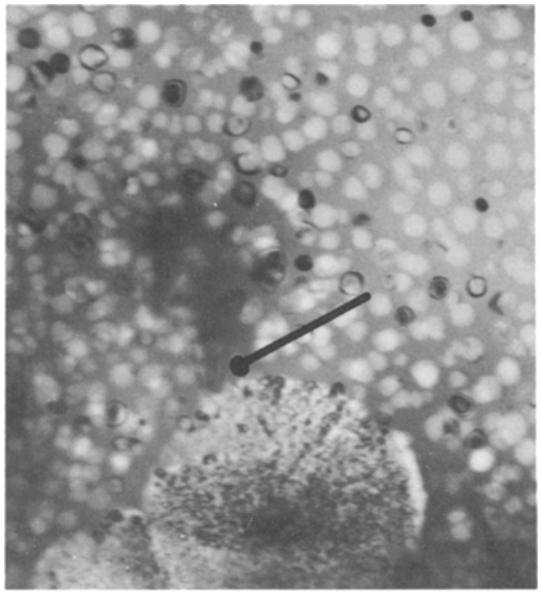

Figure 3 Same area as Fig. 1b after 20 sec at 510 K showing ϵ-phase decomposition and growth of the resulting BCT ferrite grains relative to the indicated foil imperfection (× 47 000).

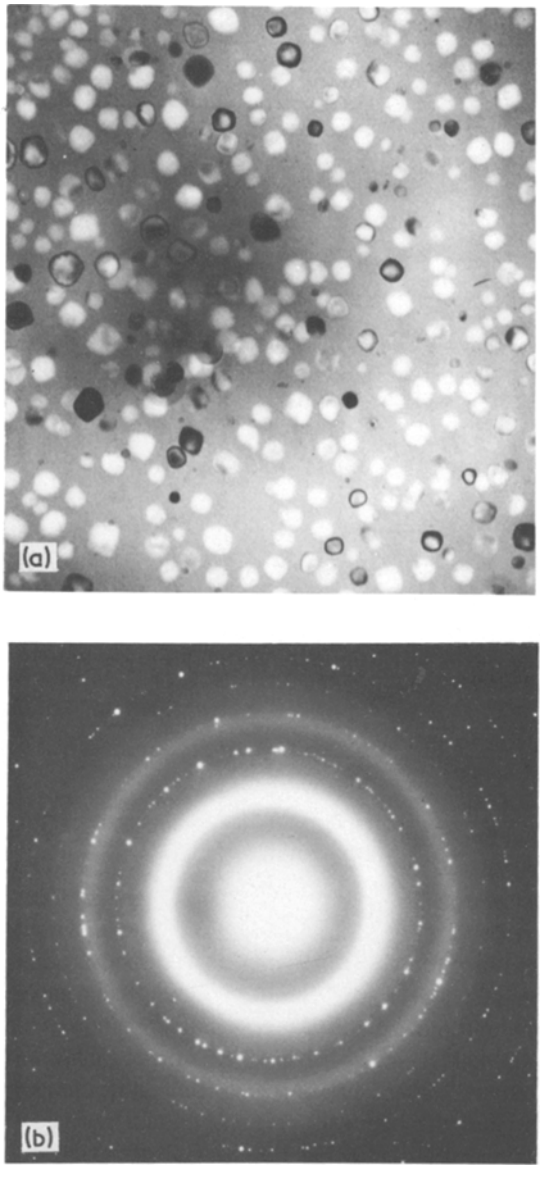

Figure 4 Typical ferrite plus amorphous phase microstructure (a) and diffraction pattern (b) obtained during the MS-I crystallization reaction after 30 sec at 510 K (× 33 000).

3.2.3.2. MS-II reaction. It was not possible to suppress the MS-I reaction so the MS-II stage consisted of a few striated grains growing in a partially crystallized mixture of the amorphous and ferrite phases. The uncrystallized material was consumed thereby leaving the ferrite crystals embedded in the striated grains. A typical microstructure taken during the MS-II reaction is given in Fig. 5 for an isothermal heat-treatment of 95 sec at 550 K. A few MS-II grains have nucleated randomly and then grown rapidly, both normal and parallel to the internal striations at a rate that is at least an order of magnitude faster (20 nm sec^{-1}) than the growth rate of the MS-I ferrite.

A detailed description of the crystal structures and grain morphologies arising during the MS-II reaction will be presented in a future communication. Briefly, the striated MS-II grains were based on twinned ferrite which may, or may not, arise with carbides. Since some of these carbides apparently possessed unreported crystal structures it is possible that structural descriptions based on complex single phase grains, rather than ferrite plus complex carbides, would be appropriate. The latter description, on the other hand, is preferred because most of the MS-II stage grains comprised cementite plates or laths, which grew co-operatively with ferrite and obeyed the Bagaryatskii [12] or possibly the Isaichev [13] orientation relationship with the parent phase. This relationship is not unexpected because it arises out of the close atomic fit between these phases [14]. It is argued that less stable crystallization structures will most likely contain more complex carbides than can also form co-operatively with the ferrite. Hence

Figure 5 Typical microstructure obtained during the MS-II reaction after 95 sec at 550 K: striated grains are observed to consume the uncrystallized amorphous material (× 59 000).

TABLE I Average d-spacings of Fe–C amorphous phases

Composition (wt %)	Total solute content (at. %)	Specimen*	d-spacing (nm)			Reference
			1st ring	2nd ring	3rd ring	
0	0	VQ	0.203	0.120	0.080	[15]
3.8C	15.52	LQ	0.203	0.192	–	[1]
1.9Si, 4.2C	19.90	LQ	0.204	0.121	–	[16]
6.0P, 1.7C	14.40	LQ	0.207	0.123	0.090	[17]
$\simeq$4.3	$\simeq$17.3	LQ	0.205 ±.002	0.121 ±.002	0.085 ±.002	present work

*VQ: vapour quenched, measured at 4.2 K; LQ; liquid quenched, measured at 300 K.

the MS-II stage predominantly involves the nucleation and growth of two-phase grains of ferrite plus various carbides.

4. Discussion

4.1. The amorphous phase

The non-crystalline phase examined in this investigation is thought to be truly amorphous because (a) it crystallized rapidly over a narrow temperature range, (b) the grain growth of microcrystals was not observed and (c) it gave a characteristic electron diffraction pattern. This characteristic pattern contained a shoulder on the second peak which is a commonly observed feature of patterns arising from metal–metalloid glasses. In the absence of a detailed radial distribution analysis it is impossible to determine whether the amorphous phase has the same structure as similar material produced in a Fe–3.8 wt % C alloy [1]. However, reference to Table I, which gives reported values of the average 'd-spacings' of the diffuse rings of diffracted intensity for amorphous Fe–C phases, indicates that material under investigation must be structurally related to Fe [15], Fe–3.8 wt % C [1], Fe–4.2 wt % C–1.9 wt % S [16] Fe–1.7 wt % C – 6 wt % P [17] amorphous phases. In the present case, the d-spacings were obtained using a camera constant that has been determined from the diffraction patterns of external (polycrystalline aluminium) and internal (the MS-I ferrite) standards.

Examination of Table I also indicates that the addition of 3.8 wt % C to pure Fe appears to have little effect on the average d-spacings of the first and second rings. However, the errors in these values are of the same order of magnitude as the increase that would be expected on the basis of the observed increase of average d-spacings with increasing P content in Ni–P amorphous alloys [18]. The amorphous phase examined in this investigation most likely contained more than 3.8 wt % C because it gave larger average d-spacings than those reported for an amorphous phase of this nominal composition [1].

Thermal analysis conducted during the decomposition of glasses on heating generally gives a temperature for the initiation of crystallization, T_c, which is a measure of the stability of the glass [19]. Comparisons between estimates of T_c and isothermal time–temperature–transformation diagrams for the crystallization of $Pd_{80}Si_{20}$ [10], $Pd_{781}Si_{164}Cu_{55}$ [20] and $Fe_{80}P_7C_{13}$ [11] glasses show that T_c corresponds approximately to the temperature required for the initation of the MS-I reaction within about 60 sec. Hence the temperature (480 K) above which MS-I crystallization occurred within a few minutes in this investigation, probably represents a good estimate of T_c for the Fe–C alloy. On the other hand, Shingu *et al.* [1] observed rapid transformation of an Fe–3.8 wt % C amorphous phase during beam heating. The temperature rise due to beam heating is approximately 100 K [21] so the T_c of their material is about 390 K. The higher T_c observed in this study probably reflects a marked increase in T_c with increasing carbon content. It has been argued that ordering systems of the Fe–C type, with their strong tendencies for the formation of intermediate compounds give an increase in T_c with increasing metalloid concentration and this view is supported by experimentally determined values of T_c for PtNiP amorphous alloys [5]. Consequently, considerations of thermal stability also indicate that the material under investigation has more than 3.8 wt % C. Furthermore, T_c variations in a given binary system of the Fe–C type probably reflect changes in the melting point [5] which would be 75° K on increasing the carbon concentration from 3.8 wt % C to 4.3 wt % C, the composition of the alloy with the lowest equilibrium melting point. A large proportion of the observed

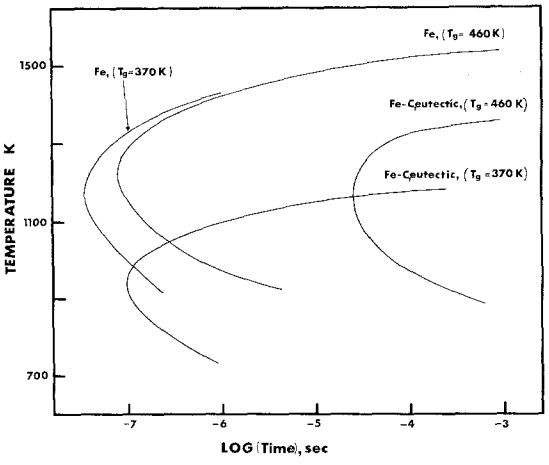

Figure 6 Calculated time–temperature–transformation curves for an undetectable amount of crystallization from the liquid in pure Fe and eutectic Fe–4.3 wt % C alloys.

T_c increase of 480–390 = 90 K would be accounted for by this 75° K melting point change so it is likely that the alloy composition is 4.3 ± 0.5 wt % C.

4.2. Cooling rates for the formation of an amorphous phase in Fe–C alloys

In view of the fact that an amorphous phase can be obtained in Fe–C alloys over a range of carbon concentrations, it is of interest to calculate the required undercoolings and cooling rates for glass formation in these alloys. The two thermal parameters can be calculated from accepted nucleation theories [4] by constructing a time-temperature-transformation curve for an undetectable amount of crystallization (usually 10^{-4}% by volume). The necessary cooling rate is given by dividing the undercooling at the "nose" of the curve by the transformation time at this temperature. Fig. 6 gives T–T–T curves for pure Fe and a Fe–4.3 wt % C alloy that were calculated from the parameters detailed in Table II. The most critical parameters required were reasonable estimates of the glass transition temperatures, T_g, for the two materials. It is generally observed in metallic glasses that $T_c = T_g + 25$ (± 25) K so likely T_g values for 3.8 and 4.3 wt % C amorphous phase are 370 ± 25 K and 460 ± 25 K. A lower limit for the T_g of the eutectic alloy was assumed to be the likely T_g of the 3.8 wt % C material while an upper limit for T_g of pure Fe is taken to be the likely T_g for the 4.3 wt % C material. These two case (Fe–4.3 wt % C, T_g = 370 K; Fe, T_g = 460 K) probably represent limiting situations and more realistic estimates are given by increasing and decreasing T_g respectively.

Referring to Table II it can be seen that the calculated cooling rates and undercooling for glass formation for pure Fe (T_g = 460 K) and eutectic Fe–C (T_g = 370 K) are almost the same and that decreasing T_g by 90 K in the case of pure Fe has little effect. There is, however, a very marked decrease in the cooling rates and undercoolings that must be achieved in order to suppress detectable crystallization in the eutectic alloy on in-

TABLE II Critical cooling rates for glass formation in Fe–C alloys and the assumed property values

	0 wt % C		4.3 wt % C	
Critical cooling rate (K sec^{-1})	7×10^9	2×10^{10}	5×10^9	1×10^7
Critical undercooling (K)	590	640	485	255
Glass transition temp. T_g (K for $\zeta = 10^{13}$ P)	460 (this investigation)	370	370 [1]	460
Melting temp. (K)	1810		1425	
Latent heat (kJ mol^{-1})	15.20 [22]		8.940 [23]	
Viscosity	extrapolated [24, 25]		extrapolated [25]	
Atom diameter (nm)	0.248		0.257	
No. atoms m^{-3}	8.4×10^{28}		10.4×10^{28}	
Vol. fraction transformed	10^{-6}		10^{-6}	
Fraction of sites	1		1	

creasing T_g by 90 K to 460 K. In this case the required cooling rate (1×10^7 K sec^{-1}) is obtained under Newtonian cooling conditions in electron transparent regions (thickness = 0.15 μm) if the heat transfer coefficient is greater than 6×10^3 J m^{-2} K^{-1} sec^{-1}. This is a very reasonable value [26] that can probably be achieved without elaborate splat-cooling procedures provided quenching is conducted in a vacuum.

Ruhl [27] has shown that the average cooling rate from the melting point to 1100 K of a 0.1 μm thick Fe splat on a copper substrate held at room temperature is 8×10^{11} K sec^{-1} so the calculated cooling rates are probably attainable for wide ranges of T_g and carbon concentrations.

4.3. Crystallization of the amorphous phase

The crystallization reactions of Fe-based amorphous phases on heating, such as the transformations reported in the present work, have been examined by few investigators. Shingu *et al.* [1] observed the formation of unidentified phase or phases on beam heating their Fe–3.8 wt % C alloy; Rastogi [28] described equiaxed, dendritic, spherulitic and cellular grains in an FeCP alloy; and Masumoto and Kimura [11] determined a T–T–T diagram for the MS-I and MS-II reactions on heating an amorphous $Fe_{80}P_{13}C_7$ phase. None of these investigators have related the formation temperatures of the various crystallization products to likely glass transition temperatures.

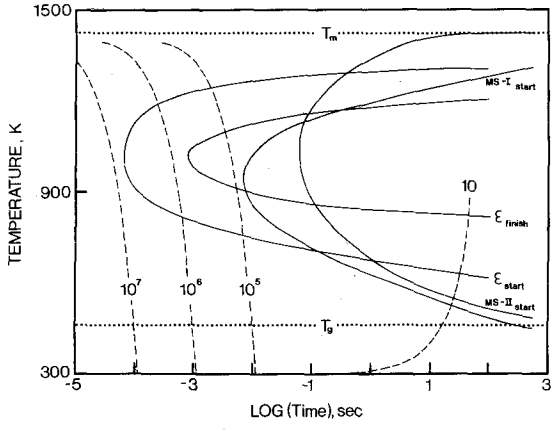

Figure 7 Schematic time–temperature–transformation curves (solid lines) for the independent nucleation and growth of metastable ϵ, MS-I and MS-II crystallization products in a supercooled Fe $\simeq$ 4.3 wt % C liquid alloy. Dashed lines indicate linear cooling and heating curves that are representative of the experimental conditions used (rates given in K sec^{-1}).

The crystallization characteristics of some other metallic glasses have been described in more detail. In particular, two stage reactions have also been observed in $Pd_{80}Si_{20}$ [3] and $Pd_{781}Si_{164}Cu_{55}$ [20] alloys. In both these systems, as well as in the $Fe_{80}P_{13}C_7$ alloy referred to above, the first stages (MS-I) involved the formation of small grains of the terminal solvent-rich solid solution. However, the structures developed during the subsequent MS-II stages have only been systematically investigated in the $Pd_{781}Si_{164}Cu_{55}$ alloy [20] and in this case, one of the MS-II reaction products was observed to comprise two-phase grains with a regular microstructure. The origins of the frequency observed striations of MS-II grains that nucleated and grew in the $Pd_{80}Si_{20}$ and $Fe_{80}P_7C_{13}$ alloys have only been discussed in general terms [3].

4.3.1. Crystallization structures developed on heating the Fe $\simeq$ 4.3 wt % C amorphous phase

The Fe $\simeq$ 4.3 wt % C ($Fe_{83}C_{17}$) alloy under investigation crystallized by a two-stage reaction. The first (MS-I) stage corresponded to the formation of the terminal, solvent-rich phase, namely ferrite, while striated grains nucleated and grew during the subsequent MS-II stage. There were no indications of segregation effects, such as phase separation prior to MS-I formation or solute rejection during the growth of this phase, which can lead to the transformation of the amorphous phase to another non-crystalline phase [19, 29]. The MS-II reaction products were generally found to be composed of ferrite grains containing a regular arrangement of cementite lamellae or laths. More complex structures could also be detected and these were probably cellular in nature but made up of other metastable carbides plus ferrite. Comparisons between the ferrite–cementite cells formed during crystallization and conventional martensitic structures arising from the transformation of austenite are not appropriate and in fact, the former are analagous to the structures produced by cellular solidification reactions: this is also likely to be the case for the more complex MS-II crystallization products.

4.3.2. Temperature ranges of the crystallization reactions

The MS-I and MS-II crystallization reactions were only observed on heating the as-quenched amorph-

ous $Fe_{83}C_{17}$ alloy to temperatures between T_g + 20 (± 35) K and T_g + 90 (± 35) K. Products of neither reaction could be detected in as-quenched foils that had been splat-cooled under the experimental conditions employed here.

On the other hand, the ϵ-phase could only be found in as-quenched foils and it did not nucleate or grow on heating the amorphous phase to temperatures between T_g + 20 (± 35) K and T_g + 90 (± 35) K under the present experimental arrangements (hot stage heating in the electron microscope). The observation of ϵ-phase in conjunction with the amorphous phase in splat-cooled foils could imply that it crystallized from the amorphous phase as a result of local reheating or, that it crystallized from the melt during quenching. The former possibility can in principle, occur as a consequence of heat removal from subsequently deposited material through previously formed amorphous regions. This process could heat the amorphous phase to temperatures that led to ϵ-phase formation. However, microstructures, such as that shown in Fig. 1b, containing ϵ-phase grains embedded in the amorphous matrix are unlikely to have arisen through extremely localised reheating. Consequently, it is reasonable to suppose that the ϵ-phase crystallized from the liquid on quenching.

These observations could be interpreted according to the conventional argument [5, 30] that unspecified factors, and by implication structure and transformation characteristics, are different for the eutectic Fe–C liquid or, indeed, for any splat-quenched liquid, in the direct cooling and reheating temperature regions. However, there is no evidence for a thermal history dependence on the structure of supercooled liquids, upon which the conventional argument relies. As an alternative proposition, it is suggested that the differences in microstructures developed on down- and up-quenching are due to the relative dispositions of the crystallization reactions on T–T–T curves. It is possible to construct approximate T–T–T curves for the independent nucleation and growth of metastable phases such as ϵ, MS-I and MS-II and to superimpose a set of cooling curves that adequately describe the thermal histories of splat-cooled foil areas, as is shown in Fig. 7. In the present case, if the start and finish curves for the ϵ-phase crystallization are displaced to short times relative to the corresponding curves for the MS reactions, then only the ϵ-phase would normally arise in conjunction with the amorphous phase on down-quenching. On the other hand, ϵ-phase crystallization on heating the amorphous phase would require very high heating rates in order to avoid the MS transformation curves. This would account for the observation that it was apparently impossible to nucleate the ϵ-phase on heating the amorphous phase due to the limited heating rates used (less than 10 K sec^{-1}).

5. Conclusions

(1) A simple splat-cooling procedure, involving controlled carburization and quenching in a vacuum, has enabled an amorphous phase to be produced in Fe–C alloys.

(2) From measured average d-spacings of selected-area diffraction patterns, the amorphous material that could be repeatedly obtained was shown to have an estimated carbon concentration of approximately 4.3 wt % C.

(3) ϵ-phase, a single phase h c p solid solution, was sometimes observed in conjunction with the amorphous phase in as-quenched foils.

(4) Upon reheating, the $Fe \simeq 4.3$ wt % C amorphous phase decomposed via a characteristic two-stage, MS-I and MS-II reaction sequence. The first stage (MS-I) involved the formation of equiaxed ferrite crystals while the second stage (MS-II) corresponded with the independent nucleation and growth of striated grains usually comprising a periodic arrangement of ferrite and cementite.

(5) The experimental observations were explained in terms of the nucleation and growth kinetics of the different metastable phases as reflected in T–T–T curves.

Acknowledgement

The authors are indebted to the Australian Research Grants Committee for supporting this research.

References

1. P. H. SHINGU, K. KOBOYASHI, K. SHIMOMURA and R. OZAKI, *Scripta Met.* 8 (1974) 1317.
2. H. A. DAVIES, J. ANCOTE, and J. B. HULL, *ibid* 8 (1974) 1179.
3. T. MASUMOTO and R. MADDIN, *Acta Met.* 19 (1971) 725.
4. D. R. UHLMANN, *J. Non-Cryst. Solids* 7 (1972) 337.
5. H. S. CHEN, *Acta Met.* 22 (1974) 1505.
6. M. C. RUHL and M. COHEN, *Trans. Met. Soc. AIME* 245 (1969) 241.

7. H. JONES, *J. Phys. D. (Appl. Phys.)* **4** (1971) 1657.
8. A. R. MARDER and G. KRAUSS, *Trans. ASM* **60** (1967) 651.
9. G. S. CARGILL, III, *Sol. Stat. Phys.* **30** (1975) 227.
10. T. MASUMOTO and R. MADDIN, *Mater. Sci. Eng.* **19** (1975) 1.
11. T. MASUMOTO and H. KIMURA, *J. Jap. Inst. Metals,* to be published.
12. YU A. BAGARYATSII, *Dokl. Adad. Neuk. SSSR* **73** (1950) 1161.
13. I. V. ISAICHEV, *Zhur, Tekhn. Fiziki* **17** (1947) 835.
14. K. W. ANDREWS, *Acta Met.* **11** (1963) 939; **12** (1964) 921.
15. T. ICHIKAWA, *Phys. Stat. Sol.* **A19** (1973) 707.
16. J. R. SARE, *Scripta Met.* **9** (1975) 607.
17. S. C. LIN and P. DUWEZ, *Phys. Stat. Sol.* **34** (1969) 469.
18. G. S. CARGILL, III, *J. Appl. Phys.* **41** (1970) 12.
19. H. S. CHEN and D. A. TURNBULL, *Acta. Met.* **17** (1969) 1021.
20. P. G. BOSWELL and G. A. CHADWICK, *Scripta Met.* **10** (1976) 509.
21. R. D. HEIDENREICH, "Fundamentals of Electron Microscopy" (Interscience, New York, 1964).
22. C. J. SMITHELLS, "Metals Reference Book", 4th Ed. (Butterworths, *London,* 1967).
23. M. HILLERT and V. V. SUBA RAO, "The Solidification of Metals" (Iron and Steel Institute, London, 1967) p. 204.
24. Y. OGINO, Z. MIRITA and A. ADACHI, *Osaka Univ. Tech. Rep.* **71** (1971) 339.
25. W. KRIEGER and H. TRENKLER, *Arch. Eisenhuttenw.* **42** (1971) 685.
26. H. JONES, *Rep. Prog. Phys.* **36** (1973) 1425.
27. R. C. RUHL, *Mater. Sci. Eng.* **1** (1967) 313.
28. P. K. RASTOGI, *J. Mater. Sci.* 8 (1973) 140.
29. J. M. VITEK, J. B. VANDER SANDE and N. J. GRANT, *Acta Met.* **23** (1975) 165.
30. S. TAKAYAMA, *J. Mater. Sci.* **11** (1976) 164.

Received 5 January and accepted 4 May 1976.